Experimental report

07/09/2022

Proposal: 5-31-2884 **Council:** 4/2021

Title: Investigating magnetostriction in super-hard epsilon-Fe2O3 polymorph

Research area: Materials

This proposal is a new proposal

Main proposer: Jose Luis GARCIA MUNOZ

Experimental team: Naureen KHANAM
Arnau ROMAGUERA CAMPS
Jose Luis GARCIA MUNOZ
MARTI GICH-GARCIA

Local contacts: Clemens RITTER
Oscar Ramon FABELO ROSA

Samples: epsilon-Fe2O3

Instrument	Requested days	Allocated days	From	To
D20	3	2	11/09/2021	13/09/2021

Abstract:

Epsilon-Fe2O3 presents a complex non-centrosymmetric Pna21 magnetically frustrated structure. It displays functional properties such as huge coercivity, millimeter-wave ferromagnetic resonance, non-linear magneto-optical effect, magnetoelectric coupling, multiferroicity at room temperature, and rich magnetic and magnetostructural properties that are very poorly understood. It is one of the less studied ferrimagnetic iron oxides due to its difficult preparation. The main objective of this experiment under magnetic field is to gain insight on the magneto-structural mechanisms that give rise to the unique super-hard ferrimagnetic phase (FM2) in this exotic trivalent iron oxide.

Experimental Report

Proposal number: 5-31-2884
Title: Investigating magnetostriction in super-hard epsilon-Fe2O3 polymorph
Instrument: D20
Experimental Team: Jose Luis GARCIA MUÑOZ (main proposer), Martí GICH GARCIA, Naureen KHANAM, Arnau ROMAGUERA CAMPS
Local Contact: Clemens RITTER, Oscar Ramon FABELO ROSA
Date: 11/09/2021 - 13/09/2021

Abstract:

Epsilon-Fe2O3 presents a complex non-centrosymmetric $Pna2_1$ magnetically frustrated structure. It displays functional properties such as huge coercivity, millimeter-wave ferromagnetic resonance, non-linear magneto-optical effect, magnetoelectric coupling, multiferroicity at room temperature, and rich magnetic and magnetostructural properties that are very poorly understood. It is one of the less studied ferrimagnetic iron oxides due to its difficult preparation. The main objective of this experiment under magnetic field is to gain insight on the magneto-structural mechanisms that give rise to the unique super-hard ferrimagnetic phase (FM2) in this exotic trivalent iron oxide.

Report:

Measurements were made on ε-Fe_2O_3 samples between 10K-300K using a cryomagnet providing magnetic fields up to 6T. Wavelengths 1.54 and 2.41 Å were employed, the former providing excellent resolution of the magnetic reflections at low q, and the latter a wider q-range for structural study. For the isothermal loops, 40 min patterns were collected at different magnetic field values using the scanning detector mode, in which a total of 40 patterns of 60 sec collected along a Theta-scan (-8<Θo<-6, step 0.05º) were merged for signal-to-noise ratio enhancement. In the case of variable-temperature measurements, 10 min simple acquisitions using the fixed detector mode were collected in dynamic mode by means of temperature ramps with heating rates of 0.75 K/min.

Due to the nanoparticle powder nature of the samples, it was necessary to overcome the possible appearance of preferred orientation caused by the reorientation of the powder grains under the application of magnetic fields. It is very important to avoid this effect in order to obtain reliable data from which we aim detecting magnetostrictive effects by Rietveld refinement of the nuclear intensities. With this purpose, for the measurements within the low temperature range 10K-130K, the ε-Fe_2O_3 sample (named 'NAP1') was immersed into deuterated isopropanol (2-Propanol-d_8 99.5 atom % D, Sigma-Aldrich) which was frozen on cooling, in order to prevent reorientation of the nanoparticles under the application of magnetic fields. To avoid crystallization of the isopropanol, which freezes around T~115 K in a glassy state, the liquid solution was loaded into a cylindrical vanadium holder, mounted on the stick, and rapidly cooled at zero field inside the cryomagnet. For the measurements at temperatures above the freezing point of deuterated isopropanol, we prepared a second sample (named 'MGG3') in which the ε-Fe_2O_3 nanoparticles were embedded in an amorphous silica matrix. In this sample, each grain contains hundreds of randomly oriented ε-Fe_2O_3 nanoparticles, thus reducing a lot the possibility of preferred orientation effects due to magnetic field application. Additionally, a cadmium cylinder was used to keep the powder tight inside the vanadium container.

First of all, field-dependent measurements were done on the MGG3 sample at the super-hard (FM2, 150K<T<500K) magnetic regime. Using λ=1.54 Å, 11 fixed-temperature patterns at 300 K were collected along H: 0T→5T with steps of 0.5T. A monotonous increase of the magnetic reflection intensities of the commensurate magnetic (CM) phase was observed, without field-induced magnetic transitions detected up to 5 T. However, from the Rietveld analysis of the structure we expect to find evidence of atomic shifts under magnetic field that can give insights on the origin of the huge coercive field of the super-hard phase (analysis ongoing).

Subsequently to the measurements at room temperature, the MGG3 was replaced by the NAP1 sample with isopropanol and cooled in zero field to proceed with the study of the effects of magnetic field in the low temperature incommensurate magnetic (ICM) phase (T<100 K) magnetic regime. For that, isothermal variable-field loops were collected

at various temperatures (10 K, 20 K, 55 K and 75 K). For 20 K and 55 K, wavelength 1.54 Å was employed to collect 40 min patterns along a H: 0T→5T→0T cycle with steps of 0.5T. The measurements reveal that the ICM phase with magnetic propagation vector $\mathbf{k}_{ICM} = [0, \delta, 0]$ undergoes an ICM to CM magnetic order transition under applied magnetic fields ranging from 0T to 1T, as it can be observed from the evolution of the magnetic intensities characteristic of the ICM magnetic propagation vector ($\mathbf{k}_{ICM}$) shown in Figs. 1(a) and 1(b) (top) at 20 K and 55 K, respectively. After this, we moved to wavelength 2.41 Å to complete the loops with more points increasing H in shorter steps to resolve better the field-induced transition. We also collected field-dependent patterns at 10 K and 75 K, in this case in a more reduced range of H, but high enough fields to observe the onset of the field-induced transition.

The amount of ICM magnetic phase decreases accordingly to an increase of CM magnetic order. However, for none of the temperatures the total transformation of the ICM into CM magnetic order is achieved at the maximum magnetic field applied (5T), as is reflected in the refined average Fe magnetic moment for the ICM and CM phases shown in Fig. 1(c). Likely, the coexistence of CM and ICM magnetic order could be attributed to the magnetic anisotropy of the ICM order. Since we have a random distribution of nanoparticle orientations, the projection of the maximum magnetic field that is effectively applied along the magnetic easy axis of each monocrystalline particle can range from 0T to 5T, thus causing a virtual coexistence of the two separated phases and a widening the magnetic transition. The onset of the field-induced transition (H_C) versus temperature, determined from each set of isothermal measurements, is shown in the inset of Fig. 1(c). We observe that the ICM phase is more stable at lower temperatures, and the critical field decreases as we approach to the ordering temperature of the incommensurate phase (AF2-ICM, T_{ICM} = 100 K). Both the magnetic and structural evolution along the ICM-CM field-induced transition will be refined and studied with further detail. These field values are in agreement with the temperature dependent coercive fields obtained from M versus H measurements (see inset of Fig. 1(c)).

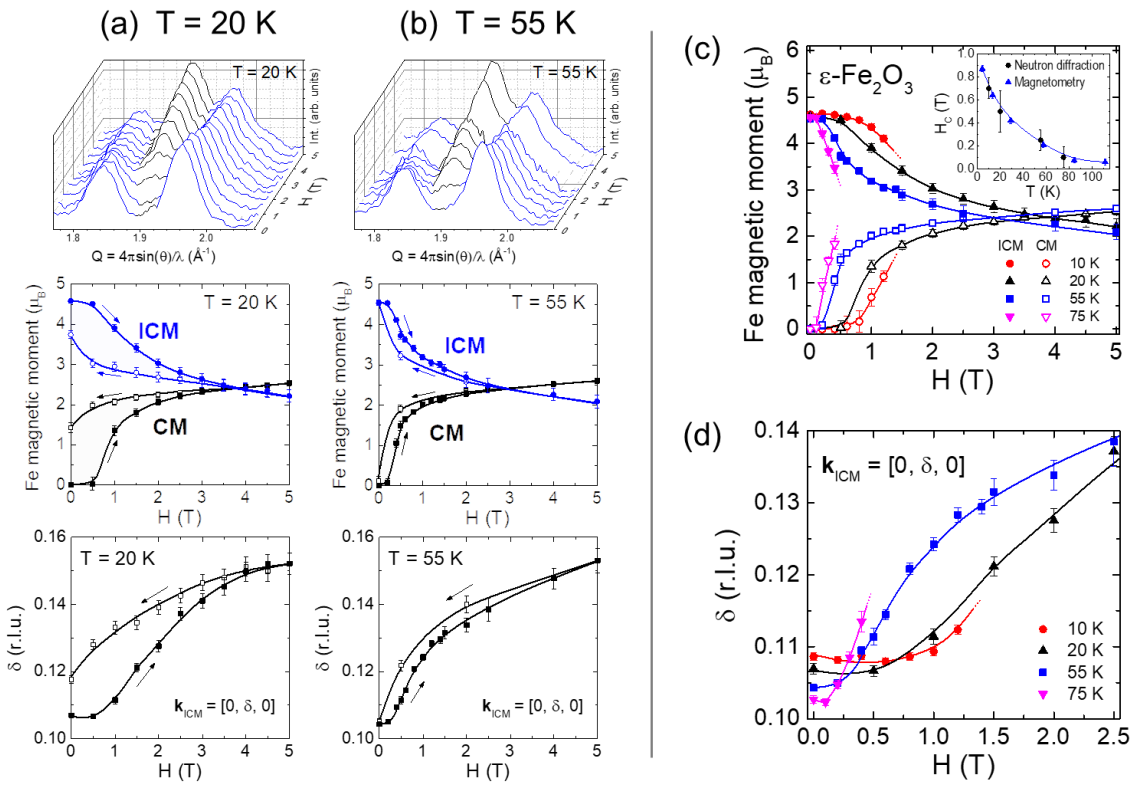

Figure 1. Field dependence of magnetic reflections characteristic of the ICM and CM phases (top), refined magnetic moment of iron (middle) for each phase, and the $k_y = \delta$ component of the ICM magnetic propagation vector (bottom) along a H: 0T→5T→0T cycle at (**a**) 20 K and (**b**) 55 K; (**c**) Refined magnetic moment for various temperatures (10 K, 20 K, 55 K and 75 K) along the ICM-CM field-induced transition (inset: temperature dependence of the critical field H_C obtained from neutron diffraction (black circles) and magnetometry measurements (blue triangles)), filled and empty points corresponding to the ICM and CM phase respectively; (**d**) Field dependence of the ICM magnetic propagation vector at 10 K, 20 K, 55 K and 75 K along the ICM-CM field-induced transition.

We also observed irreversibility of the field-induced transition. The refined magnetic moment of both phases along H: 0T→5T→0T at 20 K and 55 K, respectively in Figs. 1(a) and 1(b) (middle), show a remanence of CM magnetic order after decreasing H from 5T to 0T. This remanence of the CM phase is larger at lower temperatures, accordingly to the recovery of the coercive field below 100 K on decreasing temperature observed from magnetometry M(H) loops (see Fig. 1C of the proposal).

Additionally, the magnetic field has a noticeable effect on the magnetic wave vector of the ICM phase. Fig. 1(d) shows the magnetic modulation vector ($k_y = \delta$) refined from the Bragg position of the ICM magnetic reflections as function of the magnetic field at 10 K, 20 K, 55 K and 75 K. We observe that δ starts to increase correspondingly with the onset of the ICM-CM transition and keeps going up with the magnetic field along with the decrease of the ICM phase fraction. Figs. 1(a) and 1(b) (bottom) depicts the evolution of δ along H: 0T→5T→0T at 20 K and 50 K respectively. We see that the incommensurability of the ICM phase increases steadily from nearly δ ~ 0.10 r.l.u. at zero field up to δ ~ 0.15 r.l.u. at 5T. When the magnetic field decreases a similar irreversibility is observed as in the case of the magnetic moment.

Ultimately, a temperature-dependent measurement was conducted across the CM-ICM transition at a fixed magnetic field of 0.3 T (Fig. 2(a)). In this case, 10 min simple acquisitions were continuously collected between 16 K and 128 K following a temperature ramp of 0.75 K/min. The evolution of the magnetic phases will be analyzed and compared with similar measurements done at zero field.

No usable data could be collected above 128 K due to transformation of deuterated isopropanol. Fig. 2(b) shows the intensity evolution of the NAP1 ε-Fe2O3 sample with isopropanol along a Theta-scan with temperature drift from 130 K to 140 K, in which the apparition of a crystalline phase of the isopropanol can be observed around T~132 K. Fig. 2(c) displays the patterns of MGG3 (ε-Fe_2O_3+SiO_2) and NAP1 (ε-Fe_2O_3+Isoprop.) samples in different conditions. In the case of MGG3 (pink line), the amorphous SiO_2 gives rise to a broad bump in the data around 2θ ~ 22º. Similarly, the glassy state of frozen isopropanol in NAP1 sample gives a weak and wide bump around 2θ ~ 21.5º (blue line). Above 130 K, the crystalline phase of isopropanol appears (red line) until it eventually melts (green line) and the bump appears at lower 2θ values.

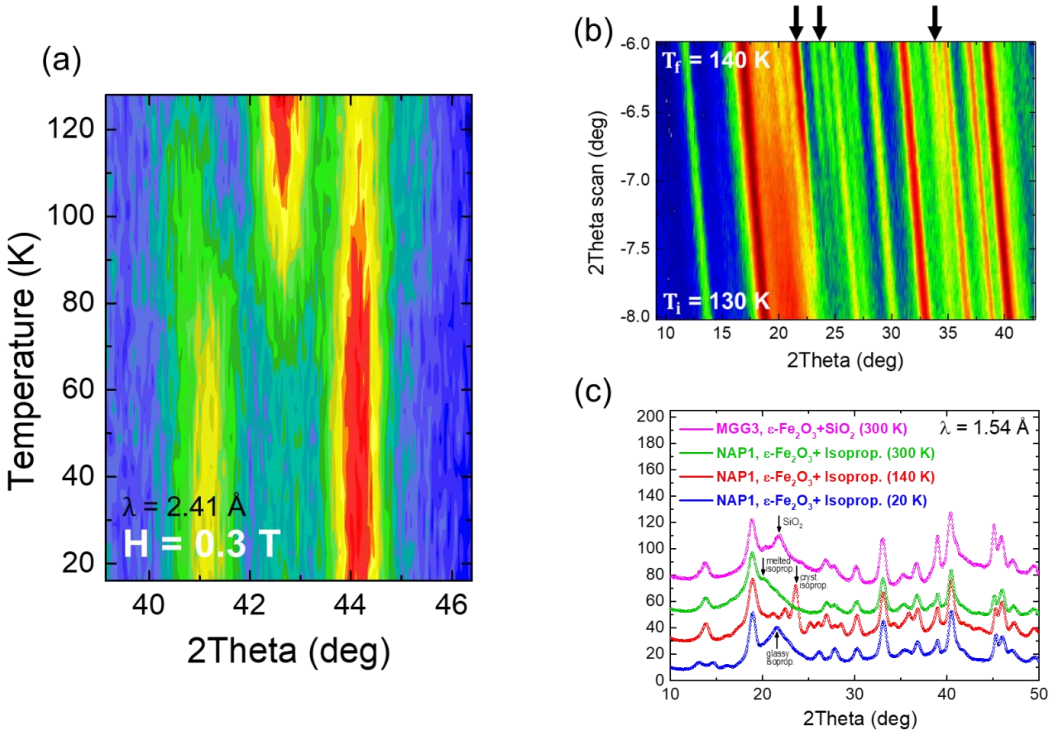

Figure 2. (**a**) 2D contour plot showing the temperature dependence of the magnetic reflections measured under H=0.3T; (**b**) Intensity evolution of the NAP1 ε-Fe_2O_3 sample with isopropanol along a Theta-scan with temperature drift in which the apparition of a crystalline phase of the isopropanol can be observed above T~132 K. Black arrows show the crystalline isopropanol peaks; (**c**) Diffraction patterns of MGG3, showing the amorphous SiO_2 background, and NAP1 sample with isopropanol at different temperature conditions showing different states of the isopropanol.